

Dynamically tunable mirrors for THz free electron laser applications

M. Tecimer,¹ K. Holldack,² and L. R. Elias¹

¹*University of Hawaii at Manoa, THz-FEL Group, Honolulu, Hawaii 96822, USA*

²*Helmholtz-Zentrum Berlin, Elektronenspeicherring BESSY II, 12489 Berlin, Germany*

(Received 21 January 2010; published 31 March 2010)

We have constructed and tested 1D-photonic crystal (PhC) mirrors with tunable reflectivity to be used as efficient, broadband outcouplers for THz free electron lasers (FELs). The test mirrors cover a spectral range between 0.5 and 1.5 THz. They are assembled by stacking up quarter-wave dielectric layers separated by vacuum. The adopted PhC mirror design enables dynamical (while lasing) adjustment of individual layer spacing. Single as well as multiple defects in the periodicity are introduced to invoke a continuous, well-defined tuning of reflectivity and outcoupling ratio. The scheme allows one to vary also the PhC period while the equidistant spacing between the layers is maintained. This feature is used to shift the photonic band gap (center) for achieving an effective extension in the reflectance spectrum. Because of the exceptional flexibility provided by the scheme in tailoring the characteristics of the PhC defects, additional features such as tunable (narrow) bandpass filtering as well as (fast) THz intensity modulation can be combined with the reflectivity/coupler properties of the proposed PhC mirrors for FELs.

DOI: [10.1103/PhysRevSTAB.13.030703](https://doi.org/10.1103/PhysRevSTAB.13.030703)

PACS numbers: 41.60.Cr, 07.57.Hm, 42.79.Fm, 42.72.Ai

I. INTRODUCTION

Outcoupling efficiency is a crucial parameter in defining the peak and average free electron laser (FEL) power available for user experiments as well as reducing the heat load deposited on the resonator structure in high power FEL systems. While the commonly used metallic mirror “hole” outcouplers offer a relatively simple means of broadband outcoupling in the THz region, their efficiency remains low at $\sim 50\%$ [1]. The remaining part of the radiation power dissipates by mode conversion as Ohmic loss into the mirror/waveguide assembly. Previously, within the frame of a THz FEL design study [2,3], we have proposed the use of intracavity (silicon) beam splitters as outcouplers [4] to alleviate the problem. However, in view of superior tuning characteristics and ease of operation, a study has been initiated to examine also the possibility of adopting low-loss dielectric multilayer [Bragg or 1D photonic crystal (PhC)] structures as outcoupler and high reflectivity mirrors for the construction of high- Q THz cavities [3]. Because of the nearly 100% outcoupling efficiency provided by these PhC reflectors, the outcoupled THz FEL pulse energy (power) can be doubled as compared to the widely used hole-type outcouplers. In addition, the negligible mode distortion (uniform coupling ratio across the beam cross section) achieved at the coupling makes them also an ideal coupler type for injecting the generated FEL pulses into an external THz pulse stacker cavity [3,5]. Since THz FELs are high power radiation sources, it is imperative to employ low-loss materials within the cavity; chemical vapor-deposited (CVD) diamond (D), high resistivity (~ 10 k Ω cm) silicon (Si), and z-cut crystalline quartz (Q) are considered due to their low (power) absorption $\{\alpha < 0.03$ cm $^{-1}$ [D and Si (10 k Ω)], $\alpha \sim 0.02$ – 0.20 cm $^{-1}$ (Q)} and a high

index of refraction ($n_{\text{Si}} = 3.41$, $n_D = 2.37$, $n_Q = 2.11$) over the THz range of interest [6–8].

One-dimensional PhC mirrors have been constructed and tested for experiments in the THz spectroscopy previously [9–11]. The schemes presented in the current study introduce several novel aspects [12,13]: a fine (0.1% tuning accuracy), continuous tuning of reflectivity is accomplished by adjusting the interlayer spacing (single or multiple layers). The reflection/transmission characteristics of a 1D-PhC mirror are otherwise fixed due to a few, discrete number of low-loss dielectric layers used in its assembly. Overcoming this limitation, the studied scheme opens up a practical way to establish the broadband 1D-PhC mirrors for applications in THz FELs that are known to be continuously tunable devices over a large spectral range. It allows online adjustment of a well-defined coupling ratio at a given frequency within the high reflectivity band (photonic band gap) in order to optimize the FEL performance. Owing to the flexibility offered by the scheme in tailoring the optical properties of the PhC defects, features such as tunable (narrow) bandpass filtering as well as (fast) THz intensity modulation can be combined with the above-mentioned reflectivity/coupler characteristics. The latter creates new means of manipulating the intracavity buildup process in THz FELs as well as postprocessing the temporal/spectral properties of the generated intense THz FEL pulses [3,13]. In addition, the ability of varying the basic unit cell size (while employing the same dielectric wafers) helps to extend the operational reflectivity band of the PhC mirror, by nearly doubling it.

II. METHOD

A schematic layout of a THz FEL that employs a 1D PhC mirror is illustrated in Fig. 1. Two parallel metal plates

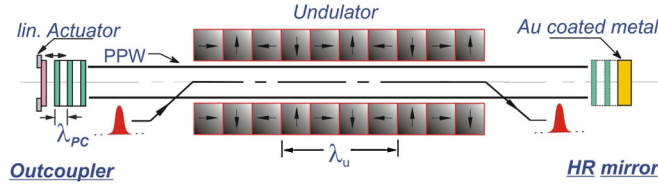


FIG. 1. (Color) Schematic layout of a PPW THz FEL employing 1D PhC outcoupler mirror. λ_{PC} and λ_u are the PhC's cell size and undulator period, respectively. A relativistic electron beam pulse is injected from the side into the PPW. Use of a metal-dielectric high-reflection (HR) mirror [31–33] is optional for a FEL cavity. In the case of an external THz pulse stacker cavity where HR mirror reflectivities in excess of 99.9% are needed, it helps to reduce the number of the cells required inside the PhC.

placed within a (planar) undulator gap and extending over the entire cavity act as a low-loss waveguide (PPW) structure allowing the excitation of hybrid (Gauss-Hermite) transverse waveguide modes [14]. The waveguided resonator comprises a metallic high reflectivity mirror and a PhC mirror providing broadband feedback and outcoupling. Figures 2(a) and 2(b) display the computed reflectance spectra of 1D PhCs formed by stacking quarter-wave, low-loss Si and z-cut quartz layers separated by vacuum. The thickness of the individual (dielectric, vacuum) layers is set to be $\lambda_C/4n$, λ_C , and n denoting the targeted central wavelength and the layer's refractive index, respectively. For the particular case of quarter-wave stack (QWS), the fractional bandwidth of the fundamental photonic band gap is maximized. It is given by [15]

$$\frac{\Delta \lambda_{\text{gap}}}{\lambda_C} \cong \frac{4}{\pi} \sin^{-1} \left| \frac{n_d - 1}{n_d + 1} \right|, \quad (1)$$

where n_d is the refractive index of the dielectric layer. The

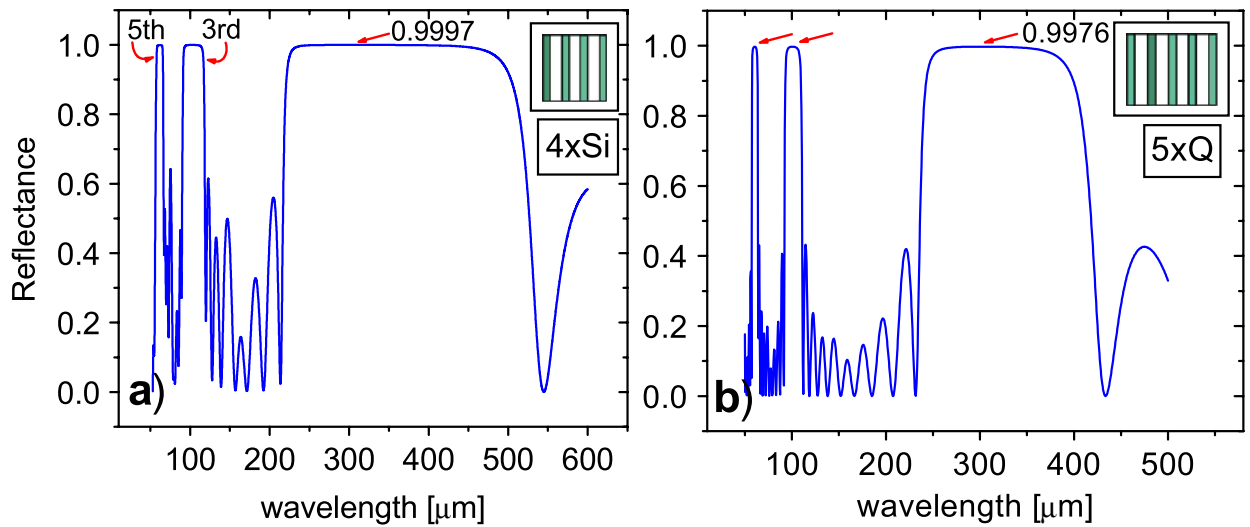


FIG. 2. (Color) In (a) four layers of 23 μm thick Si, and in (b) five layers of 36 μm thick z-cut quartz, each separated by 75 μm vacuum gap, create high reflectivity bands centered at $\lambda_C \sim 300\text{--}320 \mu\text{m}$. The harmonic band centers are located at ~ 100 and $\sim 60 \mu\text{m}$, respectively.

FEL can be tuned to operate at any wavelength λ_r within the high reflectivity band. PPW THz FELs operate typically at the fundamental mode with λ_r given by

$$\lambda_r = \frac{\lambda_u}{\gamma_z^2 \beta_z [1 + \beta_z \sqrt{1 - (\frac{\lambda_u}{2\gamma_z \beta_z g})^2}]}, \quad (2)$$

where β_z is the normalized axial velocity of the relativistic electron beam, $\gamma_z = (1 - \beta_z^2)^{-1/2}$ the longitudinal Lorentz factor, and “g” the waveguide gap. The continuous tunability of λ_r is accomplished via the beam energy and the undulator field strength which both determine the electrons' axial velocity in the beam. λ_{PC} roughly relates to the undulator period λ_u shown in Fig. 1 in a simplified relation by omitting the waveguide dispersion as

$$\lambda_{PC} \approx \lambda_u \frac{(1 + a_u^2)(1 + n_d)}{8\gamma^2 n_d}. \quad (3)$$

Here, $a_u = 0.093 \cdot B_u [\text{kG}] \cdot \lambda_u [\text{cm}]$ is the undulator parameter, B_u being the on-axis magnetic field strength of the undulator. For many THz FELs $\lambda_u (\sim 10 \text{ cm})$ is typically 3 orders of magnitude larger than λ_{PC} .

The reflectance spectra in Fig. 2 shows also the presence of (odd) harmonic photonic band gaps. Although we stress here the application to the fundamental photonic band gap, the studied tuning concept is valid for the higher harmonics as well. An important application that makes use of the third harmonic will be detailed further below.

As illustrated in Fig. 3, the online reflectivity/transmission tuning schemes, that are implemented in the tested PhC mirrors, can be categorized into three major groups regarding their functionality. The schemes shown in the first group (I.a–I.c) suit well for serving as fine-tunable

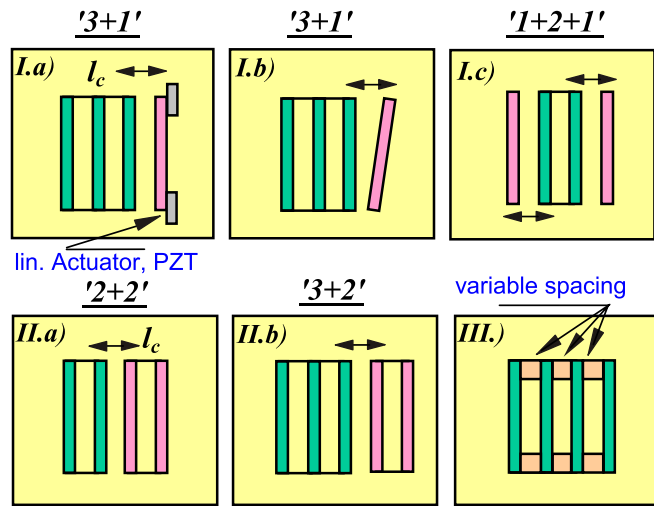


FIG. 3. (Color) Dynamic reflectivity/transmission tuning schemes. The labels above refer in the text to the respective stacking configurations.

FEL outcoupler mirrors. Introducing the reconfigurable defects shown in this first group, rather modest tuning rates ($\sim 0.1\%$ – 1% change in transmission due to a micron displacement of the movable layer) can be realized at around the desired coupling ratio. Since THz FELs are usually high gain devices, in order to be tuned to an optimum outcoupling ratio the PhC mirror's tuning range should cover transmission values reaching from 0 up to several tens of percentages. Note that the multilayer structure shown in I.a (Fig. 3) can be viewed as a thin, asymmetric Fabry-Perot (FP) etalon consisting of a high and a lower reflectivity mirror with adjustable cavity length l_c , i.e., a FP interferometer (FPI) with relatively low finesse.

As the outer layer is displaced gradually from the equidistant position and a propagating “defect mode” [15–17] is induced inside the PhC, the associated resonant transmission peak depicted in Figs. 4(a) and 4(b) sweeps across the photonic band gap, similar to tuning the peak transmission frequency ν_m in a scanning FPI according to the resonance condition $\nu_m = m \cdot c/2l_c$, where l_c is the cavity length in vacuum and the integer m is the mode order. The latter remains unity due to a subwavelength scale l_c that supports only the excitation of a single axial mode. In this example the analogy between the defect mode and the axial FP cavity mode becomes more apparent at the central frequency that fulfills the QWS condition in an unperturbed PhC. Because of the relatively low finesse values, typically needed for the described outcoupler mode, the fractional width of the transmission peak (or the reflectivity dip) $\Delta\nu_T/\nu_C \sim 10^{-1}$ shown in Fig. 4(a) turns out to be much broader than the bandwidth of the generated THz FEL pulses which has the order of $\sim 10^{-3}$ (indicated by the dashed line). All frequencies within the FEL bandwidth experience then a nearly constant outcoupling ratio as is the case for metallic hole outcoupler mirrors.

In order to introduce an extra degree of freedom for achieving the desired coupling ratio with the proper tuning rate, additional parameters of 1D PhC can be exploited. Methods such as combination of dielectric materials in composing the PhC structure [13] (i.e. refractive index variation), tilting of the outer dielectric layer a few degrees as illustrated in I.b, and creating a pair of nested (coupled) PhC cavities with individually adjustable outmost layers [12,13], as displayed in I.c, can be utilized to overcome the limitations posed by a single variable parameter in establishing the proper relation between coupling ratio and tuning rate.

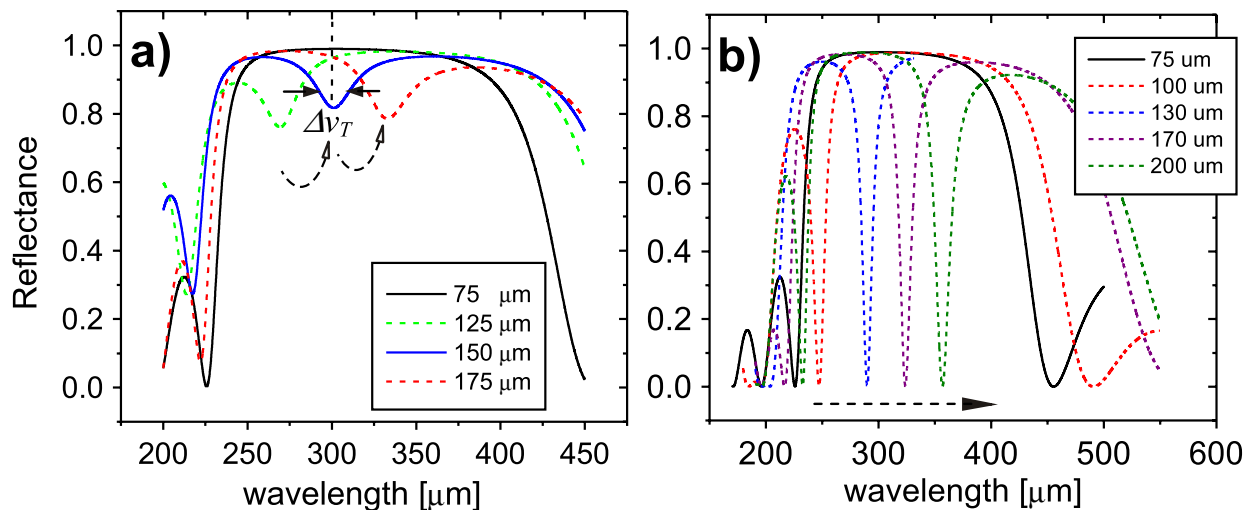


FIG. 4. (Color) Transmission peaks within the reflectivity band vs defect layer thickness. In (a) the outermost quartz wafer of a four layer stack with the sequence (3 + 1) is displaced from the equidistant position ($75 \mu\text{m}$) while in (b) the center defect layer is surrounded by two-layer stacks (2 + 2). In the latter case the fractional bandwidth of the associated transmission peak amounts to $\Delta\nu_T/\nu_C \sim 3.5 \times 10^{-2}$.

films with the same thickness deviation as for the quartz wafers. The layer assembly is enclosed between a metallic frame and a stiff, flat polished plate. Apertures centered on both pieces allow the incident radiation to propagate through the layer stack. The upper plate is tightened using small screws, exerting evenly distributed pressure on the wafer surfaces with the help of rubber strings attached to it. In the preliminary design, vacuum gap variations are first accomplished in discrete steps by employing mylar films of various gauges. In addition, continuously tunable defects are generated by means of a high-resolution stepper motor driven holder structure which accommodates the outmost layer (or bilayers), as indicated by the 3 + 1 sequence in Fig. 3-I.a.

An advanced design of current interest in our work that enables individually adjustable interlayer spacing is shown in Fig. 5. Here, the cylindrically shaped layer surfaces provide the necessary focusing of the intracavity radiation fields in the horizontal plane [14]. The radius of curvature of the mirror surfaces amounts typically to several meters.

The appeal of this design lies in the fact that the approach leads to a versatile reconfigurable, multifunctional PhC mirror which combines the features of dynamically variable outcoupling with either tunable bandpass filtering or the above-mentioned band shifting on a single, compact device that can be used to great effect in manipulating the FEL dynamics and the resulting spectral properties of the generated THz radiation. Nonetheless, the less complex, hence somewhat more robust PhC mirror approach that relies on a single actuator (or PZT transducer) as represented in Figs. 3-I and 3-II, maintains a number of the crucial tuning features and will be the focus of the presented results below.

B. Dynamical reflectivity tuning

The central wavelength λ_C of the high reflectivity bands shown in Figs. 6(a) and 6(b) is set at around $270 \mu\text{m}$ for a four and a five layer PhC mirror by assembling $31 \pm 2 \mu\text{m}$ thick quartz wafers separated by $67 \pm 2 \mu\text{m}$ vacuum gaps. The corresponding reflectivity maxima of 0.988 and 0.997

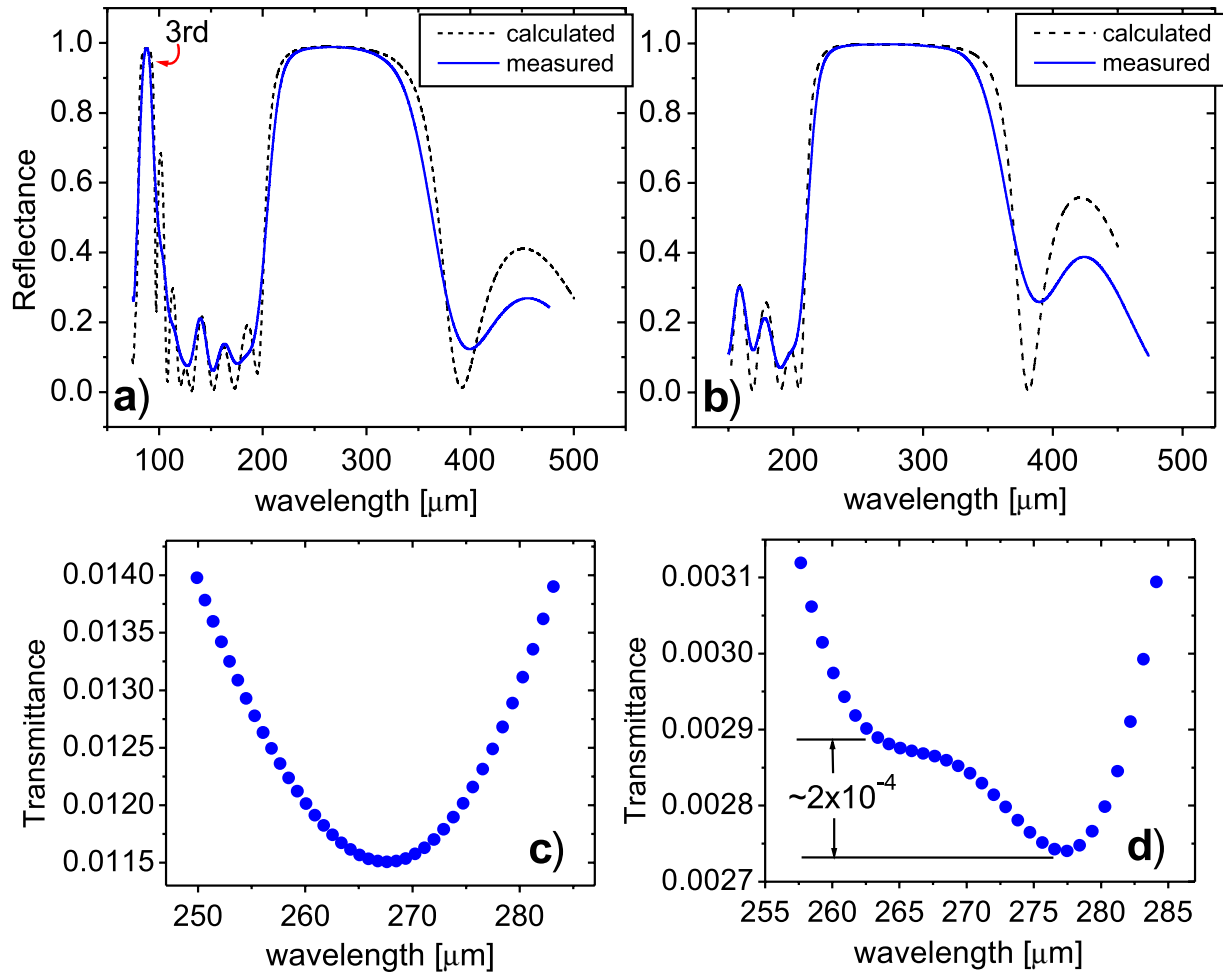


FIG. 6. (Color) Numerically calculated reflectance (dashed line) and reflectance (solid line) obtained from the measured transmittance spectra are depicted for the four layer (a) and the five layer (b) quartz PhC. The respective transmittance spectras around the band gap center are shown in (c) and (d). The asymmetric behavior present in (d) is due to a small defect arising from an imperfection in one of the quartz layers. The transmittance data of each plot is recorded with 2 cm^{-1} spectral resolution and averaged over 160 samplings.

agree closely, within $\pm 0.1\%$, with the computed ones. The achieved measurement accuracy is better than this value at the used spectral resolution [Figs. 6(c) and 6(d)]; the observed small discrepancy can be also attributed to deviations of the complex index of refraction assumed in the predictions from the actual ones. The constructed test PhC mirrors, which feature a nearly perfect periodicity, serve as the starting point for experiments to demonstrate the dynamical reflectivity tuning concept. Experimental data plotted in Fig. 7(a) contrast the reflectance spectra of the (ideal) four layer PhC mirror (blue solid curve) with the spectra generated in response to the insertion of defects (outer layer displacements and tilt). The presented sample case demonstrates the tuning capability by controlling not

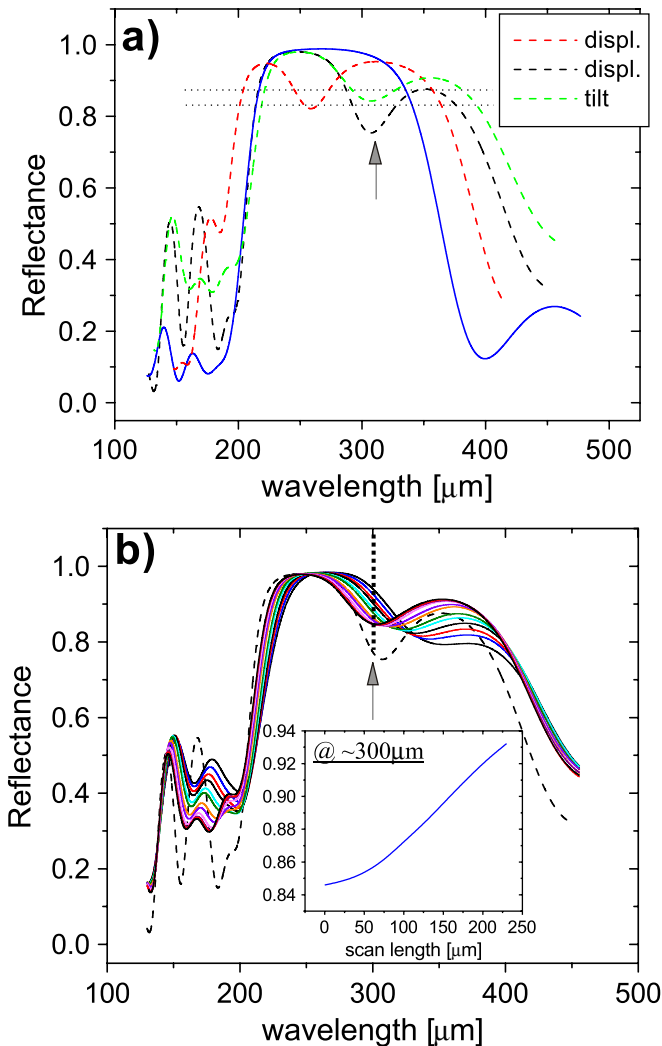


FIG. 7. (Color) (a) Measured transmission peaks created by displacing and subsequent tilting (arrow) the outermost quartz wafer (3 + 1). Fine-tuning of the outcoupling ratio is demonstrated in (b) at around $300 \mu\text{m}$ by employing a HR stepper motor driven actuator. Inset: reflectance changes obtained at a fixed wavelength (dashed line) of $\sim 300 \mu\text{m}$ as a function of the scan length.

only the position of the reflectance minima at a given wavelength but also its amplitude. The dotted lines seen in Fig. 7(a) signify the targeted range of the outcoupling ratio. One can observe that the minima of the reflectivity dip at around the desired wavelength ($\sim 300 \mu\text{m}$) turns out to drop below the targeted range by tuning only the defect layer's thickness (indicated by an arrow). By making use of an additional variable parameter (in this case by rotating the outmost quartz wafer a few degrees around the horizontal axis, as mentioned before), the minima is adjusted to the desired level while keeping its abscissa fixed [see green dashed curve in Fig. 7(a)]. Subsequent fine-tuning for a final optimization of the outcoupling ratio is carried out by positioning the outmost quartz wafer in micron steps at around the “coarsely” adjusted defect layer thickness [see Fig. 7(b)]. The induced change in reflectivity (transmissivity) at a fixed wavelength of $\sim 300 \mu\text{m}$ vs wafer displacement is shown in the inset. Here the smallest tuning rate monitored was less than $0.03\%/ \mu\text{m}$ (averaged value over a scan length of 10 microns at the vicinity of the reflectivity minima).

On the other hand, Fig. 8 displays the effect of using *refractive index variation* in two different defect layer configurations (3 + 1 and 3 + 2) as a means of introducing the additional degree of freedom. Here, the induced reflectivity change results from the displacement of the control wafer(s) with respect to the minima position at a fixed $\lambda \sim 300 \mu\text{m}$. Either single or multiple quartz wafers in the stack are replaced by the ones made of CVD diamond (*D*). Exhibiting a higher refractive index ratio, the diamond wafer (same is valid for Si wafer) enhances the resonant transmission, hence the amplitude of the reflectivity dip and invokes an opposite effect to the one induced by tilting

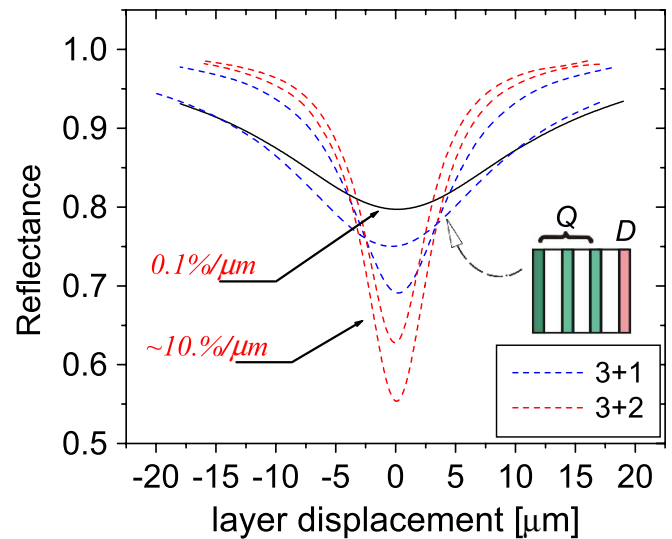


FIG. 8. (Color) Refractive index variation provides a large tuning range for setting the amplitude of the reflectivity dip at the vicinity of any THz-FEL outcoupling ratio of practical relevance. The solid curve refers to the “all quartz 3 + 1” sequence.

the control wafer. Note that, unlike other tuning schemes proposed in the study, wafer tilting has the drawback of generating a loss channel for the fundamental mode excited within the waveguided cavity; the associated decrease in the coupler efficiency, however, does not exceed a few percentages.

In terms of generating the two complementary effects mentioned above that are counteracting each other, the scheme presented in Fig. 5, which incorporates independently adjustable (outmost) layers, constitutes a more elegant way of implementing the desired flexible tuning capability. Using what we call here a *nested (coupled) PhC cavity*, at least 2 degrees of freedom are made available in manipulating the layer defects, influencing thereby interference characteristics of the multilayer structure such that the reflectance value and its slope can be controlled independently (in particular position and amplitude of the reflectance minima) at a given wavelength within the high reflectivity band. This is illustrated in Fig. 9, using a four quartz layer stack, at two different wavelengths by either increasing or reducing the value of the reflectance minima at a fixed operational wavelength. Nested PhC cavities can be also built of composite low-loss dielectrics in order to extend further the tuning capability of the PhC mirror by integrating the effect of refractive index variation, as described before.

It should be pointed out here that in the specific sample case described in Figs. 7(a) and 7(b), which was taken from a THz FEL design study [3], in view of the relatively large bandwidths of the generated transmission peaks and the associated low slope values, it suffices in practice to manipulate simply a single parameter, namely, the outmost defect layer's thickness, in order to cover the envisaged

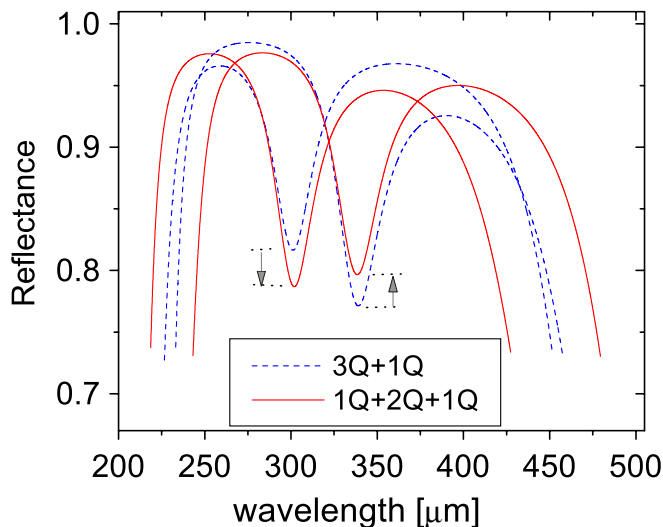


FIG. 9. (Color) Dashed curves represent the reflectivity minimas generated by the 3 + 1 configuration. Note that the latter controls only position of the reflectivity dip but not its amplitude. This task can be accomplished by using the nested PhC cavity.

range of outcoupling ratios across the entire photonic band gap. In general, however, a more sophisticated multiparameter adjustment scheme, as described above, might be necessary to meet specific requirements imposed by a FEL design.

C. Photonic band gap shifting

The central wavelength of the photonic band gap relates to the period of the PhCs employed here as $\lambda_C \approx \lambda_{PC} \cdot 4n_d/(n_d + 1)$. A spectral shift of λ_C and the respective band gap can be achieved (using the same PhC mirror and dielectric wafers) by increasing (or decreasing) the vacuum layer thickness as illustrated in Fig. 3-III). This is verified experimentally by altering the unit cell period in the five quartz layer PhC, described before [see Fig. 6(b)]. Figure 10(a) displays the measured reflectance spectra of

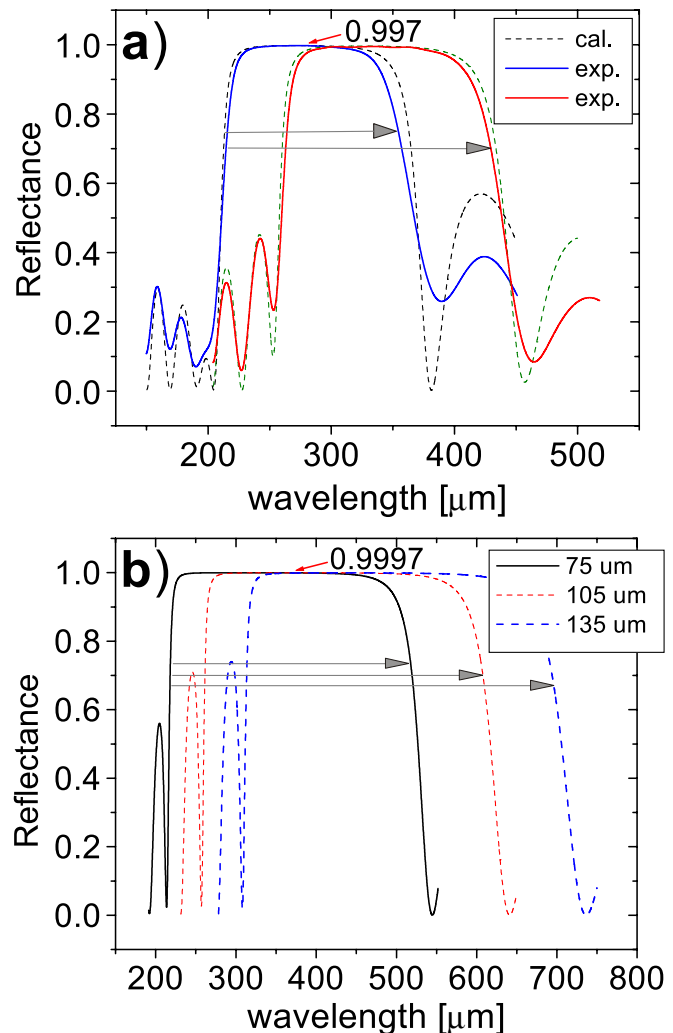


FIG. 10. (Color) Shifting high reflectivity bands as a means of extending the operational spectral range. In (a) measured and computed bands of a five layer ($\sim 31 \mu\text{m}$ thick) quartz stack. In (b) calculated spectra of a four layer $23 \mu\text{m}$ thick Si wafer stack. Vacuum spacings: 75, 105, and $135 \mu\text{m}$, respectively.

both PhCs with λ_{PC} being set to 100 and 135 μm , respectively. The measured maximum reflectance (99.7%) remains constant within $\pm 0.1\%$, noting that the altered PhC structure does not comply with the QWS condition anymore. A further increase in the gap separation up to 132 μm , i.e. $\lambda_{PC} \sim 200 \mu\text{m}$ (that had to be carried out in the preliminary design in discrete steps) led to periodicity problems arising from the relatively thick (and rigid) mylar spacers used. Figure 10(b) shows the computed band shifts achieved by employing four layer Si stacks separated by similar gap spacings as implemented in the above described quartz PhC mirror. As the shifted central wavelength increases according to the above given relation, the respective bandwidth broadens following roughly the relation given in Eq. (1). Estimations backed by the agreement obtained with the experimental data point at more than doubled operational spectral ranges (due to extensions including shifts to lower and higher frequencies) by employing a variable gap PhC mirror while the reflectance band maxima is maintained.

The practical relevance of *band shifting* that is ideally implemented in the scheme displayed in Fig. 5 is twofold. The continuous tunability offered by the currently planned and operational THz FELs over a large spectral range (typically covering 100 to 10 cm^{-1}) necessitates a broadband feedback and outcoupling mechanism. To this purpose, only a few variable gap PhC mirrors (with the respective dielectric layer thicknesses) suffice to cover the entire operational range, matching practically the broadband characteristics of widely used metallic mirrors. However, unlike the latter, variable gap PhC mirrors exhibit an exceptionally high outcoupling efficiency of nearly 100% combined with capabilities of FEL power output optimization at any operational wavelength as well as dynamically tunable narrow-band filtering. The second benefit of band shifting concerns the improvements that help to enhance the mechanical stability of the PhC mirror. In view of the relatively thin layers involved in covering particularly the short wavelength range 300 μm and below, a significant increase of layer thicknesses can be achieved by employing higher (odd) harmonic photonic band gaps, instead of the fundamental. This implies usually a trade-off between the extent of high reflectivity bands and the layer thicknesses used, as illustrated in Fig. 11. Here, fundamental bandwidth is contrasted with the third harmonic reflectivity band of a PhC mirror that is assembled by stacking 3 times thicker dielectric wafers while holding the initial gap spacing fixed. Variable gap PhCs enabling band shifting help in this case to recover the portions of the high reflectivity band that were given up otherwise for the sake of an enhanced structural stability.

D. Intracavity modulators (filters) for THz FELs

In addition to the above presented features, that have been in large verified experimentally through the built test

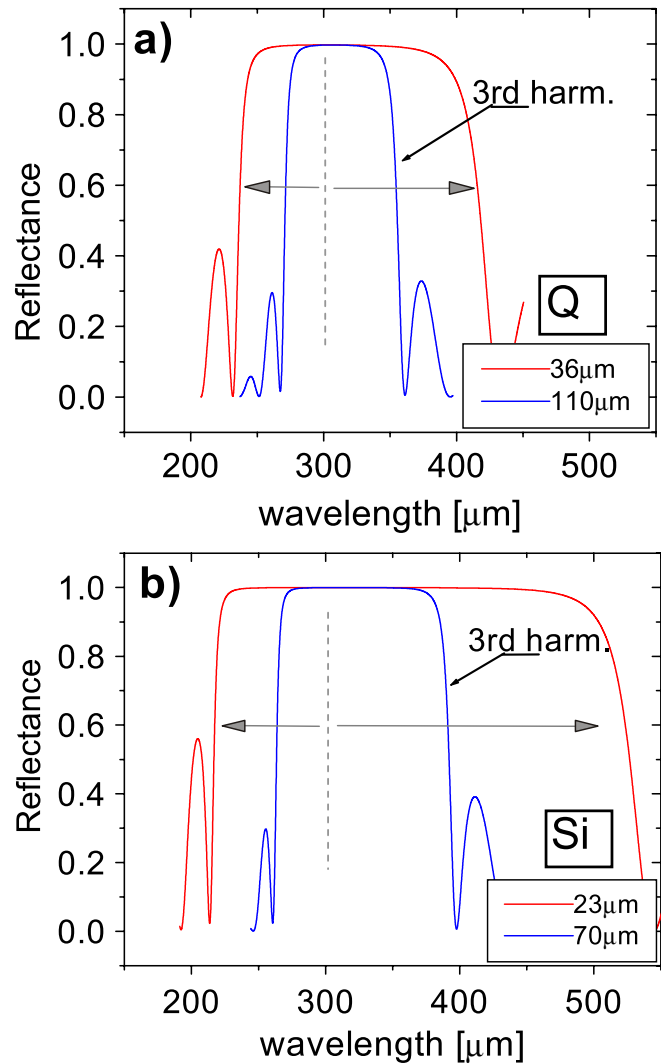


FIG. 11. (Color) Third harmonic band centers are shifted towards shorter or longer wavelengths by varying the spacing (initially 75 μm) between each quartz layer (110 μm thick) in (a) and Si layer (70 μm thick) in (b). Note that the respective fundamental HR band (not shown here) of the third harmonic band gap extends from $\sim 800 \mu\text{m}$ to well over 1000 μm for the Q PhC ($\sim 750\text{--}1300 \mu\text{m}$ for the Si PhC).

pieces, PhC mirrors with adjustable vacuum defect layers can be configured to function as tunable THz filters as well as modulators. Various approaches have been pursued to engineer tunable (electrically, magnetically, or by an external laser source optically controlled) THz filters as well as modulators/switches by using 1D and 2D PhCs [19–28]. Most notably from those approaches for the here envisaged THz FEL applications is the group which employs liquid crystals (LC) in conjunction with dielectric layers [26,27]. In fact the combination of both, individually tunable vacuum defect layers with electrically/magnetically controlled LC fillings, would enable new intriguing techniques in manipulating the temporal/spectral characteristics of the FEL buildup process. The latter approach, however, suffers

currently on the lack of (a) low-loss LC materials that are compatible with the intracavity FEL power levels and (b) that are capable of fast response times (~ 50 ns or shorter). Here, we give a brief account of the proposed THz wave modulation scheme that meets these requirements by using a simple and robust structure. The scheme will be reported elsewhere in detail along with its application on THz FELs.

As indicated in the Introduction, unlike the transmission characteristics of the defects induced for outcoupling purposes, the realization of the THz modulation requires high- Q factor defect modes inside the PhC with the associated high transmission gradients. Examples of narrow-band transmission peaks generated in a 2 + 2-type quartz stack by varying the center vacuum defect layer thickness were shown in Fig. 4(b). The transmission bandwidth of this structure is verified experimentally by measuring the spectra of a four layer PhC mirror comprising $30 \pm 2 \mu\text{m}$ thick quartz wafers with an inserted vacuum defect layer of $115 \pm 3 \mu\text{m}$. Figure 12(a) displays both, the calculated and experimental spectra for the 2 + 2 stack. In order to make the suggested method viable, however, orders of magnitude increase in the defect mode's Q factor is necessary. This can be achieved by increasing the number of cells on both sides of the defect and, at the same time, by employing dielectrics with the highest refractive index contrast. Figure 12(b) illustrates the resulting high transmission gradients attained by using a 3 + 3 Si stack (Q factor ~ 2500). Here, the central carrier frequency (~ 1 THz) is fixed by the length of the defect cavity ($\sim 150 \mu\text{m}$) introduced inside the Si PhC. The THz wave modulation frequency (~ 20 MHz) can be induced by a piezoelectric transducer that is attached on the rear side of the stack and driven by a rf signal source. On the other hand, the modulation depth is determined by the amplitude of the periodic fluctuations induced in the defect cavity length and by the slope of the resonant transmission peak. In the case of 3Si + 3Si configuration, the latter amounts to 3%–5% for 10 nm displacement. Note that sound waves propagating through the layer(s) induce both, thickness fluctuations and a change in the refraction index of the layer material, as well known from the acousto-optical effect [29]. Acoustic wave velocity of $\sim 9000 \text{ ms}^{-1}$ in Si (18000 ms^{-1} in CVD diamond) [30] supports higher modulation frequencies than the here envisaged 20 MHz and faster response times. Ideally, the PhC modulator is located at the high reflectivity mirror side (Fig. 1). At this point, it is worth to point at a more promising metal (gold) and Si layer combination which leads to a nearly order of magnitude growth in the defect mode's Q factor as compared to the mentioned 3 + 3 Si assembly while comprising a reduced number of layers in the stack (only five Si layers). The associated transmission gradients achieved by this metal-dielectric based modulator permits, despite the relatively low refractive index,

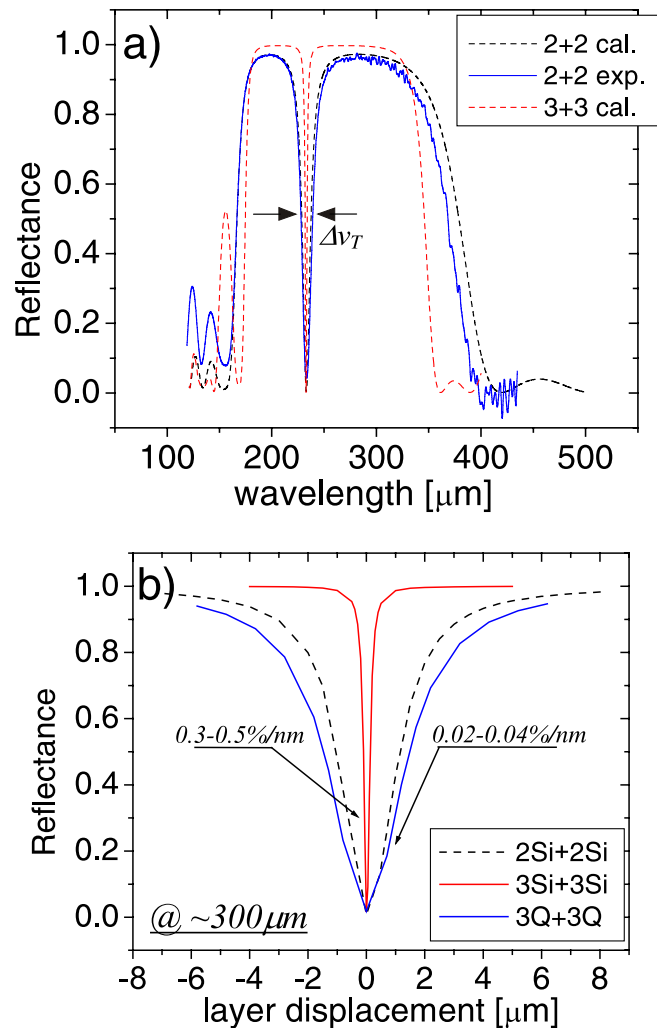


FIG. 12. (Color) Narrow transmission peaks generated by employing PhC structures of the type 2 + 2 and 3 + 3 where a defect layer is enclosed between two high reflectivity stacks. In (a), the measured fractional bandwidth (FWHM) amounts to 3.5×10^{-2} (FTIR spectral resolution: 0.1 cm^{-1}) confirming fairly well the predicted value for the 2 + 2 stack. The bandwidth is reduced further down to 9×10^{-3} using the 3 + 3 configuration. In (b), 3Q + 3Q shows the corresponding change in transmission that is induced by varying the center vacuum defect layer and keeping the wavelength fixed. In contrast, Si PhC provides an order of magnitude larger transmission gradients with the same number of cells assembled in the stack 3Si + 3Si ($\Delta\nu_T/\nu_C \sim 4 \times 10^{-4}$).

the use of quartz that inherently exhibits piezoelectric properties.

IV. CONCLUSION

The use of 1D PhCs as nearly 100% efficient, reflectivity tunable, broadband couplers is a novel concept towards achieving significant improvements in the performance of THz FELs and the related high- Q THz pulse stacker cavities. The developed scheme relies on controlling/manipulating

lating the optical properties of an FEL mirror through dynamically adjustable and versatile reconfigurable vacuum defects created inside a 1D PhC structure. While simple to implement, it is capable of addressing critical design requirements imposed by the high intracavity power levels as well as relatively large cavity-mode cross sections (many cm^2) inherent to long wavelength (rf linac or electrostatic accelerator based) THz FEL resonators. A variety of techniques [refractive index variation, nested (coupled) PhC cavities, photonic band gap shifting] are presented in the work that extend the operational capabilities of the investigated PhC coupler mirrors along with their spectral range. The use of higher harmonics in conjunction with the photonic band gap shifting constitutes a practical means to enhance the PhC's structural stability while maintaining in large functionality of the fundamental band gap. In addition to the exceptional coupler/high reflectivity characteristics, the scheme enables the implementation of tunable, narrow-band intracavity filters as well as fast modulators in THz FELs. These components can be naturally imbedded in the presented PhC mirror scheme in order to influence the FEL dynamics and to manipulate the temporal/spectral characteristics of the generated intense THz pulses. The performance of the tested PhC mirrors was crucial in verifying the computed concept and identifying the necessary improvements in the design. The next step, the practical realization of the studied PhC schemes in a THz FEL device, will demonstrate the final proof of feasibility under real life conditions.

ACKNOWLEDGMENTS

This work was supported in part by research grants from the U.S. National Science Foundation (NSF Grant No. 0520481-Subcontract No. R00916) and by the German Federal Ministry of Education and Research (BMBF, network Project No. EPR-Solar/03SF0328A/C/E). One of the authors (M.T.) would like to thank J.I. Larruquert for the useful discussions and his support in carrying out the initial simulations in the early stage of this work. We would like to thank also the BESSY accelerator group for setting up the low- α mode as well as A. Schnegg (HZB) and R. Bittl (FU Berlin) for making the Bruker IFS 125HR spectrometer available.

-
- [1] M. Tecimer, H. Jiang, and L.R. Elias, Nucl. Instrum. Methods Phys. Res., Sect. A **528**, 146 (2004).
 - [2] M. Tecimer, L.C. Brunel, J. van Tol, and G. Neil, in Proceedings of the International Free Electron Laser Conference, Berlin, 2006, p. 327.

- [3] M. Tecimer, FSU THz-FEL Design Study, Thomas Jefferson National Accelerator Facility (FEL), Newport News, July 2007; Internal Report "Multilayer Dielectric Mirrors with Enhanced Coupling Efficiency for FSU's High Q THz Cavities," FSU-NHMFL, Tallahassee, 2007; Internal Report "FIR FEL Design Results" FSU-NHMFL, Tallahassee, 2008.
- [4] E. Szarmes, Appl. Opt. **33**, 6953 (1994).
- [5] T. Smith and P. Haar, Nucl. Instrum. Methods Phys. Res., Sect. A **393**, 245 (1997).
- [6] D. Grischkowsky *et al.*, J. Opt. Soc. Am. B **7**, 2006 (1990).
- [7] J. Dai, J. Zhang, W. Zhang, and D. Grischkowsky, J. Opt. Soc. Am. B **21**, 1379 (2004).
- [8] F. Brehat and B. Wyncke, Int. J. Infrared Millim. Waves **18**, 1663 (1997).
- [9] R. Schiwon *et al.*, Appl. Phys. Lett. **83**, 4119 (2003).
- [10] T.W. Du Bosq, A.V. Muravjov, and R.E. Peale, Proc. SPIE Int. Soc. Opt. Eng. **5411**, 167 (2004).
- [11] Y. Han *et al.*, J. Korean Phys. Soc. **55**, 508 (2009).
- [12] M. Tecimer, Korea-Japan Joint Workshop on Electron Beam Applications WEBA09 KAERI, Daejeon, 2009.
- [13] M. Tecimer, K. Holldack, J.I. Larruquert, and L.R. Elias, IRMMW-THz 2009 Conference, Busan, 2009.
- [14] L.R. Elias and J.C. Gallardo, Appl. Phys. B **31**, 229 (1983).
- [15] J.D. Joannopoulos, S.G. Johnson, R.D. Meade, and J.N. Winn, *Photonic Crystals: Molding the Flow of Light* (Princeton University Press, Princeton, 2008), 2nd ed.
- [16] Y. Akahane, T. Asano, B.-S. Song, and S. Noda, Nature (London) **425**, 944 (2003).
- [17] J.-M. Lourtioz, H. Benisty, and D. Maystre, *Photonic Crystals* (Springer-Verlag, Berlin, 2008), 2nd ed.
- [18] M. Abo-Bakr, J. Feikes, K. Holldack, G. Wustefeld, and H.W. Hubers, Phys. Rev. Lett. **88**, 254801 (2002).
- [19] P. Kužel *et al.*, Opt. Lett. **30**, 549 (2005).
- [20] L. Fekete *et al.*, Opt. Lett. **32**, 680 (2007).
- [21] S.-Z. A. Lo and T.E. Murphy, Opt. Lett. **34**, 2921 (2009).
- [22] W. Withayachumnankul, B.M. Fischer, and D. Abbott, Opt. Commun. **281**, 2374 (2008).
- [23] E. Hendry *et al.*, Phys. Rev. Lett. **100**, 123901 (2008).
- [24] C.-Y. Chen, T.-R. Tsai, C.-L. Pan, and R.-P. Pan, Appl. Phys. Lett. **83**, 4497 (2003).
- [25] H. Nemeč *et al.*, J. Appl. Phys. **96**, 4072 (2004).
- [26] H. Zhang, P. Guo, P. Chen, S. Chang, and J. Yuan, J. Opt. Soc. Am. B **26**, 101 (2009).
- [27] R. Wilk, N. Vieweg1, O. Kopschinski1, and M. Koch, Opt. Express **17**, 7377 (2009).
- [28] T. Kleine-Ostmann, K. Pierz, G. Hein, P. Dawson, M. Marso, and M. Koch, J. Appl. Phys. **105**, 093707 (2009).
- [29] A. Yariv and P. Yeh, *Photonics* (Oxford University Press, New York, 2007), 6th ed.
- [30] S.-F. Wang *et al.*, Mater. Chem. Phys. **85**, 432 (2004).
- [31] M. Scalora *et al.*, J. Appl. Phys. **83**, 2377 (1998).
- [32] Y.K. Choi *et al.*, Opt. Commun. **230**, 239 (2004).
- [33] J.I. Larruquert (private communication).